

Tunable correlation effects of magnetic impurities by cubic Rashba spin-orbit coupling

Xiong-Tao Peng,¹ Fang Lin,¹ Liang Chen,² Lin Li,³ Dong-Hui Xu,^{4,5} and Jin-Hua Sun^{1,*}

¹*Department of Physics, Ningbo University, Ningbo 315211, China*

²*School of Mathematics and Physics, North China Electric Power University, Beijing 102206, China*

³*College of Physics and Electronic Engineering, and Center for Computational Sciences, Sichuan Normal University, Chengdu 610068, China*

⁴*Department of Physics and Chongqing Key Laboratory for Strongly Coupled Physics, Chongqing University, Chongqing 400044, China*

⁵*Center of Quantum Materials and Devices, Chongqing University, Chongqing 400044, China*



(Received 8 February 2023; revised 17 April 2023; accepted 18 April 2023; published 25 April 2023)

We theoretically study the influence of the k -cubic Rashba spin-orbit coupling (SOC) on the correlation effects of magnetic impurities by combining the variational method and the Hirsch-Fye quantum Monte Carlo (HFQMC) simulations. Markedly different from the normal k -linear Rashba SOC, even a small cubic Rashba term can greatly alter the band structure and induce a Van Hove singularity in a wide range of energy; thus, the single impurity local moment becomes largely tunable. The cubic Rashba SOC adopted in this paper breaks the rotational symmetry, but the host material is still invariant under the operations $\mathcal{R}^z(\pi)$, $\mathcal{I}\mathcal{R}^z(\pi/2)$, \mathcal{M}_{xz} , \mathcal{M}_{yz} , where $\mathcal{R}^z(\theta)$ is the rotation of angle θ about the z axis, \mathcal{I} is the inversion operator, and \mathcal{M}_{xz} (\mathcal{M}_{yz}) is the mirror reflection about the x - z (y - z) principal plane. Saliiently, various components of spin-spin correlation between the single magnetic impurity and the conduction electrons show three- or sixfold rotational symmetry. This unique feature is due to the triple winding of the spins with a 2π rotation of \mathbf{k} , which is a hallmark of the cubic Rashba effect, and can possibly be an identifier to distinguish the cubic Rashba SOC from the normal k -linear Rashba term in experiments. Although the cubic Rashba term drastically alters the electronic properties of the host, we find that the spatial decay rate of the spin-spin correlation function remains essentially unchanged. Moreover, the carrier-mediated Ruderman-Kittel-Kasuya-Yosida interactions between two magnetic impurities show twisted features, the ferromagnetic diagonal terms dominate when two magnetic impurities are very close, but the off-diagonal terms become important at long distances.

DOI: [10.1103/PhysRevB.107.165148](https://doi.org/10.1103/PhysRevB.107.165148)

I. INTRODUCTION

Spin-orbit coupling (SOC) is a relativistic effect that locks the spin of a charge carrier with its angular momentum, and intense efforts have been made over the past decades to investigate and utilize SOCs in condensed matter physics. There exist two representative SOCs, namely, the Dresselhaus SOC caused by the bulk inversion asymmetry [1] and the Rashba SOC due to the spatial inversion asymmetry [2,3]. In low-dimensional systems, the Rashba SOC becomes more important because it is stronger in the heterointerface [4,5], and it is often described by the k -linear Rashba term, which can be written as $\propto (k_- \sigma_+ - k_+ \sigma_-)$, where $k_{\pm} = k_x \pm ik_y$ denote the wave vectors, and $\sigma_{\pm} = \sigma_x \pm i\sigma_y$ are the spin Pauli matrices [6–8].

Remarkably different from the two-dimensional (2D) electron systems in which the k -linear Rashba SOC dominates, in 2D hole systems, the spin splitting can be third order in momentum and is usually described by the Hamiltonian $\propto (k_-^3 \sigma_+ - k_+^3 \sigma_-)$ [9–11]. The interest in this k -cubic Rashba SOC is probably triggered by the unique benefits to spin

transport predicted in such systems [12–21]. From the viewpoint of symmetry, the linear and cubic Rashba SOCs can exist simultaneously [22]. However, in some systems, the linear term can be tiny; vivid examples are strained-Ge/SiGe quantum wells [15,23] and SrTiO₃ single-crystal surface [16] and heterostructures [24–27]. The cubic Rashba SOC has also been reported in various systems such as a 2D hole gas in InGaAs and GaAs heterostructures [28,29], rare-earth ternary materials TbRh₂Si₂ [30] and EuIr₂Si₂ [31], the iridium silicide surface of GdIr₂Si₂ [32], and LaAlO₃/KTaO₃ [33] heterostructures. Density functional theory calculations show that, in bulk ferroelectric oxide PbTiO₃, the linear and cubic spin splittings coexist, and the magnitude of the linear/cubic coefficients can be tuned by applying epitaxial strain in bulk [34]. In asymmetric oxide heterostructures of LaAlO₃/SrTiO₃/LaAlO₃, a transition from the cubic Rashba effect to the coexistence of linear and cubic Rashba effects is controlled by the filling to Ti orbitals [19]. Theoretical calculations proposed that the magnitude of the linear Rashba SOC depends on the growth orientation of Ge/Si quantum wells, so purely k -cubic Rashba SOC can be realized in the [111]-oriented quantum wells when the linear term vanishes [35].

As a prototypical strong correlation problem, the Kondo effect in normal metals has been widely studied and well

*sunjinhua@nbu.edu.cn

understood [36–38]. The Kondo effect is accompanied by the formation of a Kondo cloud, which is characterized by the antiferromagnetic spin-spin correlation between the magnetic impurity and the conduction electrons. This spin-spin correlation function oscillates fast in space and decays as $\sim 1/r^D$ when $r < \xi_K$, while it decays as $\sim 1/r^{D+1}$ if $r > \xi_K$ [39–41], where ξ_K is the Kondo length that extends to $\sim 1 \mu\text{m}$ in typical metals [42], and has been confirmed recently via Fabry-Pérot oscillations in conductance [43].

The influence of k -linear Rashba SOC on the Kondo temperature T_K has been studied previously using various methods; some indicate that T_K is not significantly changed by Rashba SOC [44–46], while others claim an exponential enhancement of T_K [47,48]. Later, a numerical renormalization group study found that, for a fixed Fermi energy, the Kondo temperature T_K varies weakly with Rashba SOC. If instead, the band filling is low and held constant, increasing the Rashba SOC can drive the system into a helical regime where T_K is exponentially enhanced [49]. Basically, one important reason to change the Kondo temperature is the divergence of the density of states (DOS) which appears close to the band edge in the presence of k -linear Rashba SOC [50]. On the other hand, in 2D superconductors, it is found that T_K is determined by the interplay between the Rashba SOC and superconducting energy gap, and the quantum phase transition between the magnetic doublet and Kondo singlet ground states is significantly affected by the Rashba SOC [51].

Beyond the theoretical interest in understanding the Kondo physics in systems, the magnetic impurities can even be used to detect the properties of the host materials. For example, the Yu-Shiba-Rusinov [52–54] state induced by a magnetic impurity in a superconductor has long been a major method to characterize the pairing symmetry of the superconducting states [55–67]. In the case of systems with SOCs, it has been proposed to use a magnetic impurity as a way to detect the Rashba effect through the local magnetization DOS [68]. The hallmark of the cubic Rashba SOC is the triple winding of the spins with a complete 2π rotation of \mathbf{k} [7,30], and the spatial patterns of a Kondo screening cloud are mainly affected by the SOCs [69,70]. One can naturally expect that the Kondo screening cloud can reflect this unique property of the cubic Rashba SOC and help to identify it from the normal k -linear term. Considering the indirect exchange couplings between magnetic impurities, the Ruderman-Kittel-Kasuya-Yosida (RKKY) [71–73] couplings become twisted in the presence of SOC. The RKKY interaction in 2D systems with SOC can be written in a general form with three terms: Heisenberg, Ising, and Dzyaloshinskii-Moriya (DM) interactions, and this general form is valid for the Rashba SOC, the Dresselhaus SOC, and even when the two types of SOC are mixed [74–76].

In this paper, we combine the variational method and Hirsch-Fye quantum Monte Carlo (HFQMC) [77] simulations to study the correlation effects of the impurities induced by the cubic Rashba SOC. The variational method has been widely used in the ground states of Anderson impurity problems in normal metals [78,79], systems with SOCs [69,80–84], and superconductors [85–88]. The HFQMC technique is a numerically exact method which has been used to study magnetic impurities in metals [77,89–93], dilute magnetic

semiconductors [94], graphene-based systems [95–98], and in the presence of SOCs [99,100]. By combining the two methods, we can obtain not only a heuristic physical picture but also the numerically exact results about the correlations. The rest of the paper is organized as follows. In Sec. II, we introduce the model Hamiltonian and discuss the influence of the cubic Rashba term on the electronic properties of the host material. In Sec. III, we show the results obtained using the variational method and the Hirsch-Fye quantum Monte Carlo simulations for the single-impurity case. The spin-spin correlation between two magnetic atoms, which is mediated by the conduction electrons, is given in Sec. IV. Finally, discussions and conclusions are given in Sec. V.

II. MODEL HAMILTONIAN

We use the Anderson impurity model to study the properties of magnetic impurities in a system with the cubic Rashba SOC term; the total Hamiltonian is given by

$$H = H_0 + H_d + H_V. \quad (1)$$

Here, H_0 describes the host material with the cubic Rashba SOC, H_d is the magnetic impurity part, and H_V denotes the hybridization between the local impurities and the conduction electrons. The low-energy effective Hamiltonian of a host system with the cubic Rashba SOC is given by

$$H_0 = \sum_{\mathbf{k}} c_{\mathbf{k}}^{\dagger} [h_0(\mathbf{k}) - \mu] c_{\mathbf{k}}, \quad (2)$$

with

$$h_0(\mathbf{k}) = \frac{\hbar^2 \mathbf{k}^2}{2m} + \frac{i\alpha}{2} (k_-^3 \sigma_+ - k_+^3 \sigma_-). \quad (3)$$

Here, $h_0(\mathbf{k})$ is the single-particle Hamiltonian incorporating cubic Rashba SOC [12,15,101,102], and $c_{\mathbf{k}}^{\dagger} = (c_{\mathbf{k}\uparrow}^{\dagger}, c_{\mathbf{k}\downarrow}^{\dagger})$ is the creation operator in spinor representation. The notations $k_{\pm} = k_x \pm ik_y$, $\sigma_{\pm} = \sigma_x \pm i\sigma_y$ are used to denote the wave vectors and Pauli spin matrices, μ is the chemical potential, and α is the cubic Rashba term which can be adjusted experimentally [103–106].

The Rashba SOC is caused by the spatial inversion asymmetry of the confining potential, so it is significant in surfaces and interfaces. As we know, in a heterostructure, the charge carriers are confined in the 2D interface, and the Rashba effect depends on the gradient of the confining potential which is significant in the 2D interface. Thus, our model Hamiltonian can describe the 2D hole gases with cubic Rashba SOC in the heterostructures.

Due to the SOC, the single-particle eigenenergy splits from simple degenerate parabolic bands to two branches:

$$\epsilon_{k\pm} = \frac{\hbar^2 k^2}{2m} \pm \alpha k^3. \quad (4)$$

The magnetic impurity part is given by

$$H_d = \sum_{j,s=\uparrow,\downarrow} (\epsilon_d - \mu) d_{js}^{\dagger} d_{js} + \sum_j U d_{j\uparrow}^{\dagger} d_{j\uparrow} d_{j\downarrow}^{\dagger} d_{j\downarrow}, \quad (5)$$

where j represents the magnetic impurity index. We study two cases, namely, the single-impurity doping and the two-impurity doping. When only one magnetic impurity is doped

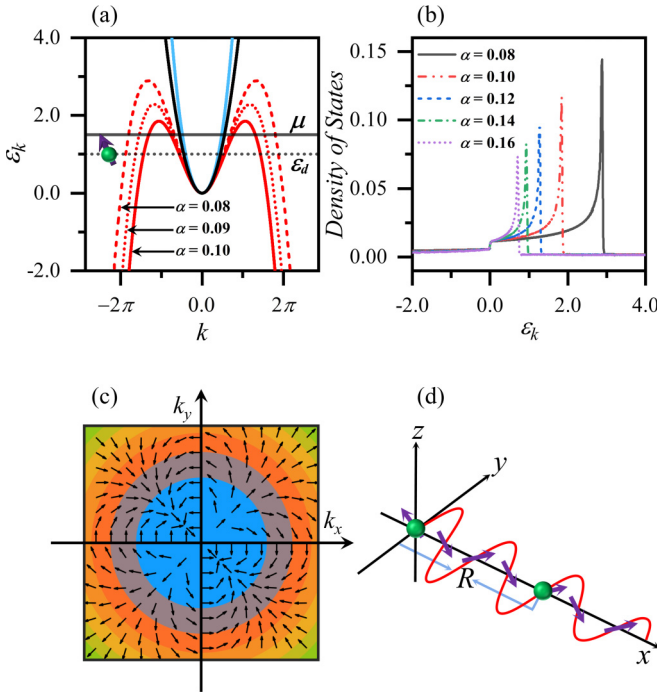


FIG. 1. (a) The twofold degenerate band (black line) splits into two bands due to the cubic Rashba spin-orbit coupling (SOC) α . The cubic Rashba term has marginal influence on the upper band (blue line). The red lines correspond to the lower bands with different α values, and they are drastically modified by α . μ is the chemical potential, and ϵ_d is the magnetic impurity energy level. (b) The density of states varies with α , and Van Hove singularity emerges. (c) Spin texture caused by the cubic Rashba SOC in momentum space. (d) Schematic of the spin-spin interaction as a function of the distance R between two magnetic impurities. The red curve means the correlation strength, and the arrows denote the rotation of spin-spin interaction due to the cubic Rashba SOC.

in the host, $j = 1$. Otherwise, if two impurities exist, $j = 1, 2$. Here, d_s^\dagger and d_s are the creation and annihilation operators of the spin- s ($s = \uparrow, \downarrow$) state on the impurity site, ϵ_d is the impurity energy level which is beneath μ in our calculations, and U is the on-site Coulomb repulsion which repels the double occupancy on the impurity site [107].

Finally, the hybridization term between the localized state and the conduction electrons reads

$$H_V = \sum_{\substack{\mathbf{k}, j, \\ s = \uparrow, \downarrow}} [\exp(i\mathbf{k} \cdot \mathbf{R}_j) V_k d_{js}^\dagger c_{\mathbf{k}s} + \text{H.c.}], \quad (6)$$

where V_k is the hybridization strength, and \mathbf{R}_j is the coordinate of the j th impurity. For two-impurity doping, we assume the two local atoms and conduction electrons have the same exchange coupling strength V_k for simplification.

In Fig. 1(a), we show the dispersion relation of the single-particle energy bands given in Eq. (3). The cubic Rashba SOC splits the degenerate parabolic band (black solid line) into two branches. One is ϵ_{k+} (blue solid line), and the other is ϵ_{k-} (red lines). The cubic Rashba SOC term has a minor effect on ϵ_{k+} , but it can alter ϵ_{k-} significantly, as we can see from the three red lines, which correspond to ϵ_{k-} for slightly different α values. The DOSs for different

α values are plotted in Fig. 1(b). The cubic Rashba term largely modifies ϵ_{k-} and consequently induces a Van Hove singularity (VHS) into the host system, which is expected to greatly influence the local moment formation of magnetic impurities. Additionally, the cubic Rashba SOC breaks the rotational symmetry, but the system remains invariant under operations such as $\mathcal{R}^z(\pi)$, $\mathcal{I}\mathcal{R}^z(\pi/2)$, \mathcal{M}_{xz} , and \mathcal{M}_{yz} , where $\mathcal{R}^z(\theta)$ is the rotation of angle θ about the z axis, \mathcal{I} is the inversion operator, and $\mathcal{M}_{xz} = \mathcal{I}\mathcal{R}^y(\pi)$ [$\mathcal{M}_{yz} = \mathcal{I}\mathcal{R}^x(\pi)$] is the mirror reflection about the x - z (y - z) principal plane, and the spin operators follow the rules $\mathcal{M}_{xz} : \{\sigma_\pm \rightarrow -\sigma_\mp\}$, $\mathcal{M}_{yz} : \{\sigma_\pm \rightarrow \sigma_\mp\}$. The spin texture given in Fig. 1(c) reflects all these symmetries, which can be exhibited by the Kondo effect. Given in Fig. 1(d) is the schematic of our two-impurity case calculation. One magnetic impurity is fixed at the origin, and the other is located at a distance R along the x axis. In our calculations, the length unit is chosen as k_0^{-1} , which in SrTiO₃ is $k_0^{-1} = a/2\pi \approx 0.6 \times 10^{-10}$ m with the lattice constant $a = 0.3905$ nm. The energy unit is $\frac{\hbar^2 k_0^2}{2m^*}$ and the values of parameters α , U , μ , V_k , and ϵ_d are given in units of $\frac{\hbar^2 k_0^2}{2m^*}$. One can use the coefficient values given in previous works [106] to find the relationship between the cubic Rashba coefficient in realistic systems and α used in our model Hamiltonian. For example, in a LaAlO₃/SrTiO₃ quantum well which is 10 nm wide, the electric field is estimated to be 1 meV/nm, and this can generate a cubic Rashba coefficient of 0.8 meV nm³. If the effective mass is chosen as $m^* = 0.5 m_0$ (m_0 is the electron rest mass), one can easily obtain that the cubic Rashba coefficient corresponds to $\alpha \approx 0.17$, which is in the same order of magnitude as is assumed in this paper.

Note that we have only considered the cubic Rashba term in the model Hamiltonian given in Eq. (3) to concentrate on the influence of the cubic Rashba SOC on the correlation effect of magnetic impurities. From the viewpoint of symmetry, once the cubic Rashba SOC appears, the linear Rashba SOC is also allowed by symmetry; thus, both SOC's can coexist [22]. However, in systems represented by strained-Ge/SiGe quantum wells [15,23] and SrTiO₃ single-crystal surface [16] and heterostructures [24–27], the linear term is negligible, and the cubic Rashba term becomes dominate, so they can be well described by the model Hamiltonian used in this paper. On the other hand, the property of the doped magnetic impurity is mainly determined by the DOS and the symmetry of the host material. Adding the k -linear Rashba SOC term in Eq. (3) will not change the symmetry of the host system; it is still invariant under the operations $\mathcal{R}^z(\pi)$, $\mathcal{I}\mathcal{R}^z(\pi/2)$, \mathcal{M}_{xz} , and \mathcal{M}_{yz} . Thus, we expect the property of the Kondo screening cloud shall remain qualitatively unchanged even in the presence of the k -linear Rashba term.

III. SINGLE-IMPURITY CORRELATION EFFECTS

A. The variational method

We can easily diagonalize H_0 and obtain a quasiparticle operator:

$$\gamma_{\mathbf{k}\pm} = \frac{1}{\sqrt{2}} \left[\exp\left(i\frac{3}{2}\theta_{\mathbf{k}}\right) c_{\mathbf{k}\uparrow} \pm i \exp\left(-i\frac{3}{2}\theta_{\mathbf{k}}\right) c_{\mathbf{k}\downarrow} \right], \quad (7)$$

where $\tan \theta_{\mathbf{k}} = k_y/k_x$, \pm denotes the upper and lower energy bands. First let us discuss the simplest case when $H_V = 0$, in which the magnetic impurity state decouples from the host material. Thus, the ground-state wave function of H_0 is given by

$$|\Psi_0\rangle = \prod_{\{\mathbf{k}\pm\} \in \Omega} \gamma_{\mathbf{k}\pm}^\dagger |0\rangle, \quad (8)$$

where $|0\rangle$ is the vacuum, and the product runs over all the states within the Fermi sea Ω . As for the impurity part, we assume that the Coulomb repulsion U is large enough, and the impurity energy level ϵ_d is below the chemical potential μ , so that the impurity site is always singly occupied by a local moment. The total energy of the system under this decoupled

case is

$$E_0 = \epsilon_d - \mu + \sum_{\{\mathbf{k}\pm\}} (\epsilon_{\mathbf{k}\pm} - \mu). \quad (9)$$

Then we consider the case with hybridization, where the trial wave function of the ground state is

$$|\Psi\rangle = \left(a_0 + \sum_{\{\mathbf{k}\pm\}} a_{\mathbf{k}\pm} d_{\mathbf{k}\pm}^\dagger \gamma_{\mathbf{k}\pm} \right) |\Psi_0\rangle, \quad (10)$$

where $d_{\mathbf{k}\pm} = \frac{1}{\sqrt{2}} [\exp(i\frac{3}{2}\theta_{\mathbf{k}})d_\uparrow \pm i \exp(-i\frac{3}{2}\theta_{\mathbf{k}})d_\downarrow]$. Here, a_0 and $a_{\mathbf{k}\pm}$ are variational parameters to be determined by optimizing the ground-state energy. The energy of the system in the trial state $|\Psi\rangle$ is given by

$$E = \frac{\langle \Psi | H | \Psi \rangle}{\langle \Psi | \Psi \rangle} = \frac{\sum_{\{\mathbf{k}\pm\}} (E_0 - \epsilon_{\mathbf{k}\pm} + \mu) a_{\mathbf{k}\pm}^2 + 2V_k a_0 a_{\mathbf{k}\pm} + (\epsilon_{\mathbf{k}\pm} - \mu) a_0^2}{a_0^2 + \sum_{\{\mathbf{k}\pm\}} a_{\mathbf{k}\pm}^2}. \quad (11)$$

The variational method requires $\partial E / \partial a_0 = \partial E / \partial a_{\mathbf{k}\pm} = 0$, leading to

$$\left[E - \sum_{\{\mathbf{k}\pm\}} (\epsilon_{\mathbf{k}\pm} - \mu) \right] a_0 = \sum_{\{\mathbf{k}\pm\}} V_k a_{\mathbf{k}\pm},$$

$$(E - E_0 + \epsilon_{\mathbf{k}\pm} - \mu) a_{\mathbf{k}\pm} = V_k a_0. \quad (12)$$

We can define the binding energy as $\Delta_b = E_0 - E$; then the self-consistent equation is given by

$$(\epsilon_d - \mu) - \Delta_b = \sum_{\{\mathbf{k}\pm\}} \frac{|V_k|^2}{\epsilon_{\mathbf{k}\pm} - \mu - \Delta_b}. \quad (13)$$

If $\Delta_b > 0$, the hybridized state is stable against the decoupled state. In our variational method calculations, the impurity energy level is fixed slightly below the chemical potential, $\epsilon_d = \mu - 0.001$, and the energy cutoff Γ is chosen to be far away from μ , so that the low-energy physical properties will not be affected by the choice of Γ .

We show the self-consistent results of the binding energy Δ_b for various combinations of V_k , μ , and α in Fig. 2. In Fig. 2(a), we show the binding energy with respect to the cubic Rashba term α for different values of V_k when $\mu = 1.85$. Here, α greatly alters the band structure and thus the DOS, as is shown in Fig. 1. We find that Δ_b shows a peak around $\alpha = 0.1$. This is because, for $\alpha = 0.1$, the VHS occurs close to the chemical potential $\mu = 1.85$. Additionally, Δ_b is larger for stronger hybridization strength V_k , implying that the bound state is more easily formed for strong V_k . In Fig. 2(b), we fix $V_k = 0.2$ and show similar results for various values of μ . The energy corresponds to the VHS decrease monotonically with α , and in a wide range of μ , we can always observe the peak of Δ_b . Figure 2(c) shows the results of Δ_b vs V_k for different combinations of μ and α . In general, Δ_b is always positive due to the finite DOS in this system, and this is consistent with the previous results obtained using the same method [69,80,81]. Larger values of Δ_b imply that the bound state is more stable. When $\alpha = 0.10$, the VHS lies around $\mu = 1.85$, such that

the binding energy Δ_b (the blue straight line) becomes much larger than other cases.

Next, we study the effect of the cubic Rashba SOC on the correlation between the local spin and the conduction electrons spins. This spin-spin correlation function measures the spatial Kondo screening cloud. The spin operator of the magnetic impurity spin is defined as $\mathbf{S}_d = \frac{1}{2} \sum_{s,s'} d_s^\dagger(\hat{\sigma})_{s,s'} d_{s'}$, and the conduction electron spin is $\mathbf{S}_c(\mathbf{r}) = \frac{1}{2} \sum_{s,s'} c_s^\dagger(\mathbf{r})(\hat{\sigma})_{s,s'} c_{s'}(\mathbf{r})$, where $s, s' = \uparrow, \downarrow$ and $\hat{\sigma} = \{\sigma_x, \sigma_y, \sigma_z\}$. By assuming the magnetic impurity location as the origin $\mathbf{r} = 0$ and the conduction electron position as \mathbf{r} , the spin-spin correlation function is given by

$$J_{uv}(\mathbf{r}) = \langle S_c^u(\mathbf{r}) S_d^v(0) \rangle, \quad (14)$$

where $\langle \dots \rangle$ is the ground state average, and $u, v = x, y, z$ are the spin indices. Here, $J_{uv}(\mathbf{r})$ can be calculated by using the trial wave function in Eq. (10).

The diagonal and the off-diagonal terms take the forms:

$$J_{zz}(\mathbf{r}) = -\frac{1}{8} |B(\mathbf{r})|^2 + \frac{1}{8} |A(\mathbf{r})|^2,$$

$$J_{xx}(\mathbf{r}) = -\frac{1}{8} |B(\mathbf{r})|^2 - \frac{1}{8} \text{Re}[A(\mathbf{r})]^2,$$

$$J_{yy}(\mathbf{r}) = -\frac{1}{8} |B(\mathbf{r})|^2 + \frac{1}{8} \text{Re}[A(\mathbf{r})]^2,$$

$$J_{xy}(\mathbf{r}) = -\frac{1}{8} \text{Im}[A(\mathbf{r})]^2,$$

$$J_{xz}(\mathbf{r}) = \frac{1}{4} \text{Im}[B(\mathbf{r})A(\mathbf{r})],$$

$$J_{yz}(\mathbf{r}) = -\frac{1}{4} \text{Re}[B(\mathbf{r})A(\mathbf{r})], \quad (15)$$

where $A(\mathbf{r}) = \sum_{\{\mathbf{k}\pm\}} \pm \exp[i(\mathbf{k} \cdot \mathbf{r} + 3\theta_{\mathbf{k}})] a_{\mathbf{k}\pm}$ and $B(\mathbf{r}) = \sum_{\{\mathbf{k}\pm\}} \exp[i\mathbf{k} \cdot \mathbf{r}] a_{\mathbf{k}\pm}$. Due to the phase factors of $\gamma_{\mathbf{k}\pm}$ given in Eq. (7), $A(\mathbf{r})$ contains the phase factor $3\theta_{\mathbf{k}}$ and thus becomes threefold rotational symmetric about the z direction, while $B(\mathbf{r})$ is isotropic in the x - y plane.

In Fig. 3, we plot the spatial patterns of the spin-spin correlation function $J_{uv}(\mathbf{r})$ ($u, v = x, y, z$), and k_c is the momentum cutoff chosen with respect to the energy cutoff Γ . Here, $J_{zz}(\mathbf{r})$ given in Fig. 3(a) is always isotropic about the origin, while $J_{xx}(\mathbf{r})$ and $J_{yy}(\mathbf{r})$ given in Figs. 3(b) and 3(c) are anisotropic because of the SOC in the x - y plane. We find

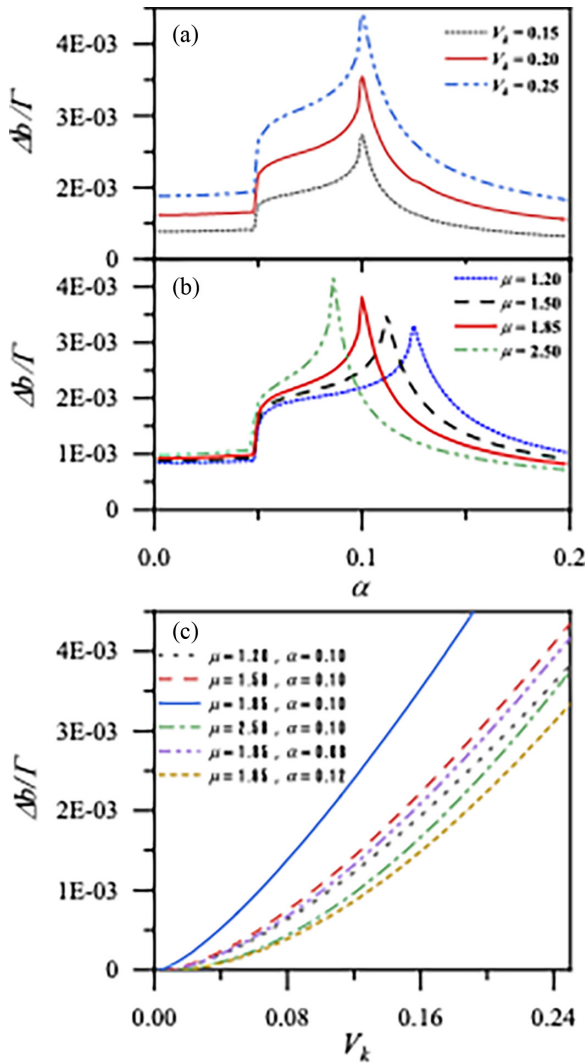


FIG. 2. Self-consistent results of the binding energy Δ_b for different combinations of parameter values. Δ_b vs α for (a) different V_k when $\mu = 1.85$ and (b) different μ when $V_k = 0.20$. (c) Δ_b vs V_k for various combinations of μ , α . Γ is the energy cutoff chosen to be far away from μ .

that the diagonal components $J_{xx}(\mathbf{r})$ and $J_{yy}(\mathbf{r})$ have threefold rotational symmetry about the z direction. Note that the host system given in Eq. (2) is not threefold rotational symmetric. However, due to the phase factors of eigenstates given in Eq. (7), the components of spin-spin correlation function show unique rotational symmetry. In addition, the host system is invariant under $\mathcal{R}^z(\pi)$, and consequently, $J_{xx}(\mathbf{r})$ and $J_{yy}(\mathbf{r})$ also satisfy the sixfold rotational symmetry. All the diagonal terms are negative around $r = 0$, indicating the antiferromagnetic coupling between the magnetic impurity spin and the conduction electron spins. The off-diagonal terms are merely induced by the SOC, and we find that $J_{xy}(\mathbf{r}) = J_{xy}(-\mathbf{r})$ in Fig. 3(d), which can be analyzed using the $\mathcal{R}^z(\pi)$ symmetry of the host material. The other two off-diagonal components have the properties $J_{xz}(x, y) = -J_{xz}(-x, y)$ and $J_{yz}(x, y) = -J_{yz}(x, -y)$. Except for the isotropic $J_{zz}(\mathbf{r})$, all the components of spin-spin correlation show either three- or sixfold rotational symmetry on the x - y plane. The underlying reason

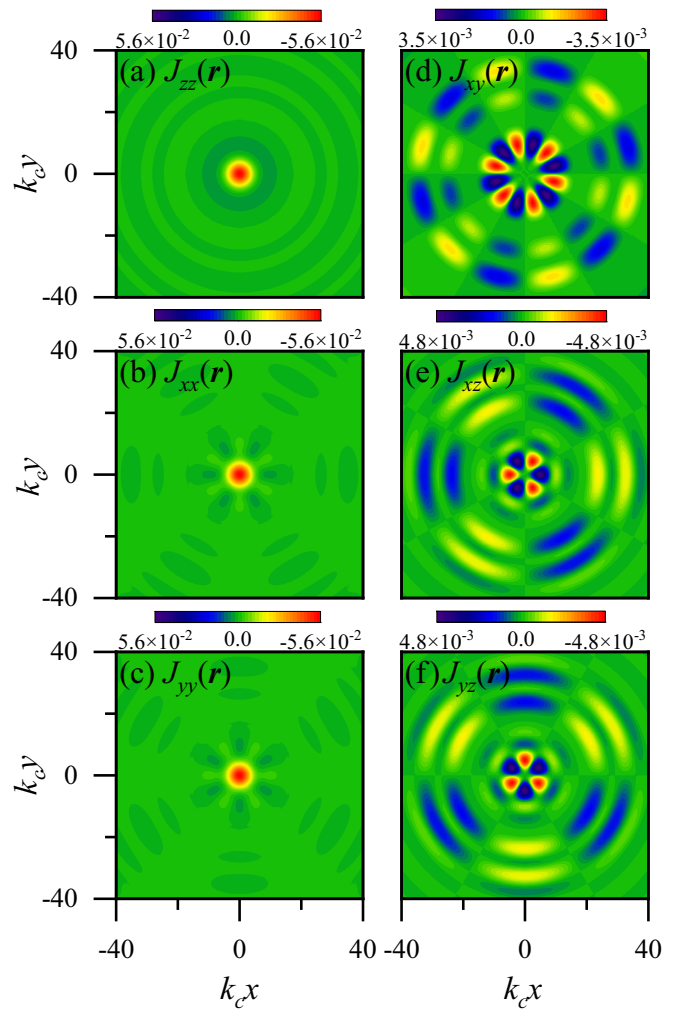


FIG. 3. The spatial pattern of the spin-spin correlation between magnetic impurity and conduction electrons with ($\alpha = 0.1$). (a) $J_{zz}(\mathbf{r})$, (b) $J_{xx}(\mathbf{r})$, (c) $J_{yy}(\mathbf{r})$, (d) $J_{xy}(\mathbf{r})$, (e) $J_{xz}(\mathbf{r})$, and (f) $J_{yz}(\mathbf{r})$. The parameters are $\Delta_b = 0.02$, $\alpha = 0.10$, $V_k = 1.0$, and $\mu = 1.50$. k_c is the momentum cutoff chosen with respect to the energy cutoff Γ .

for these unique symmetries is the triple winding of the spins with a complete 2π rotation of \mathbf{k} [7,30], which is a hallmark of the cubic Rashba effect, and can possibly be an identifier to distinguish the cubic Rashba SOC from the normal k -linear Rashba term in experiments.

All the components of the spin-spin correlation function oscillate and decay in space. To analyze the spatial decay rate of the correlations, in Fig. 4, we show the diagonal components of the spin-spin correlation function along the x axis. The parameters are chosen as $\Delta_b = 0.02$, $\alpha = 0.10$, $V_k = 1.0$, and $\mu = 1.50$. Here, $J_{zz}(\mathbf{r}) = J_{xx}(\mathbf{r}) \neq J_{yy}(\mathbf{r})$ along the x axis. Shown in the subfigure is the result of $r^2 J_{uu}(\mathbf{r})$ ($u = x, y$) along the x axis. According to previous studies, the spin-spin correlation between the magnetic impurity and the conduction electrons decays as $\approx 1/r^{D+1}$ if $r > \xi_K$ [39–41], where ξ_K is the Kondo length. However, our variational calculations support a $1/r^2$ decay for finite α at long distances. Even for the simple 2D electron gas (2DEG) with $\alpha = 0$, the decay rate of the spin-spin correlation function is still proportional to

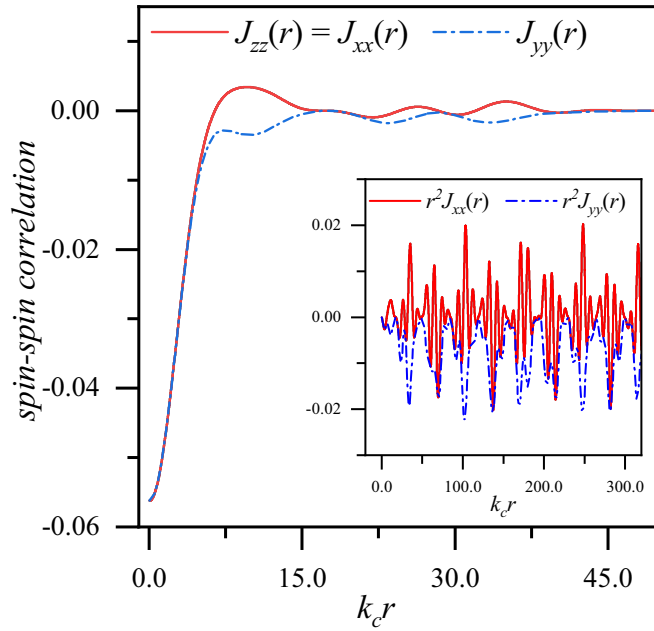


FIG. 4. Diagonal components of the spin-spin correlation functions $J_{uu}(\mathbf{r})$. The subfigure shows that the spin-spin correlation decays as $\propto 1/r^2$ along the x axis. The parameters are the same as those in Fig. 3.

$1/r^2$ unless $\Delta_b > 0.2$, which is unrealistically larger than the results of Δ_b obtained in Fig. 2. We presume this is caused by the limitation of the variational method, and it is necessary to perform the unbiased HFQMC simulations to get more accurate results.

B. Quantum Monte Carlo simulations

The basic strategy of the Hirsch-Fye algorithm is to transform the Coulomb interaction term in Eq. (5), which is quartic in operators, into quadratic terms. In this process, the interacting fermion problem is replaced by the problem of electrons coupled to an auxiliary Ising field. Various expectation values are obtained from the quantum Monte Carlo importance sampling of this auxiliary field [77,93,108]. The Hirsch-Fye algorithm naturally returns the imaginary-time Green's functions $g_{dd}^{ss'}(\tau) = -\langle T_\tau d_s(\tau) d_s^\dagger \rangle$, $G_{cd}^{ss'}(\mathbf{r}, \tau) = -\langle T_\tau c_{\mathbf{r}s}(\tau) d_s^\dagger \rangle$, $G_{dc}^{ss'}(\mathbf{r}, \tau) = -\langle T_\tau d_s(\tau) c_{\mathbf{r}s'}^\dagger \rangle$, and $G_{cc}^{ss'}(\mathbf{r}, \tau) = -\langle T_\tau c_{\mathbf{r}s}(\tau) c_{\mathbf{r}s'}^\dagger \rangle$, where $s, s' = \uparrow, \downarrow$. In the HFQMC simulations, $\langle \dots \rangle$ means taking the average over the discrete auxiliary field. Here, τ is the imaginary time range from 0 to β . All the information about the host material is included in the input noninteracting Green's functions ($U = 0$) which can be obtained analytically. By using the Green's function returned from the HFQMC simulations, we can calculate various quantities such as the expectation values of the total charge:

$$n_d = \langle n_{d\uparrow} + n_{d\downarrow} \rangle,$$

the local moment squared:

$$m_d^2 = \langle (n_{d\uparrow} - n_{d\downarrow})^2 \rangle,$$

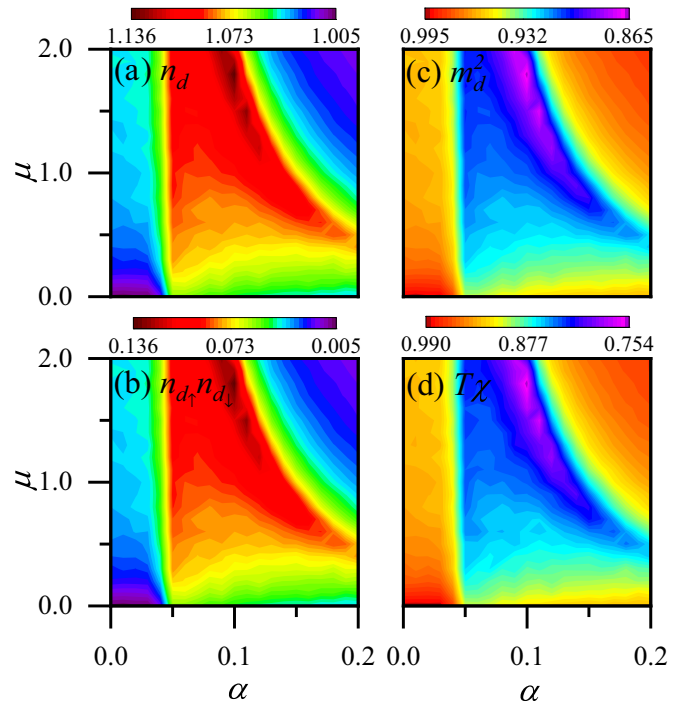


FIG. 5. The Hirsch-Fye quantum Monte Carlo (HFQMC) results of (a) n_d , (b) $n_{d\uparrow} n_{d\downarrow}$, (c) m_d^2 , and (d) $T\chi$ for various values of the chemical potential μ and the cubic Rashba term α . We choose $U = 0.8$, $V_k = 1.0$, and the temperature is $k_B T = \frac{1}{32}$.

the double occupancy:

$$n_{d\uparrow\downarrow} = \langle n_{d\uparrow} n_{d\downarrow} \rangle,$$

and the spin susceptibility:

$$\chi = \int_0^\beta d\tau \langle [n_{d\uparrow}(\tau) - n_{d\downarrow}(\tau)][n_{d\uparrow}(0) - n_{d\downarrow}(0)] \rangle.$$

Here, $\beta = 1/k_B T$ is the inverse temperature. Note that the local moment squared on the impurity site is given by $m_d^2 = n_d - 2n_{d\uparrow\downarrow}$; the closer this value is to one, the more fully developed the local moment is. In all our QMC simulations, we fix $\epsilon_d - \mu = -U/2$, namely, the symmetric case in which the local moment formation is favored [36].

In Fig. 5, we show the thermodynamic quantities with respect to the chemical potential μ and the strength of the cubic Rashba term α . The parameters are chosen as $U = 0.8$, $V_k = 1.0$, and the temperature is $k_B T = \frac{1}{32}$. The results for different parameter values shall remain qualitatively unchanged. As is given in Fig. 1, small values of α can drastically modify the dispersion relation and thus induce VHS. The energy corresponds to the VHS decreases as α increases, and this will influence the single magnetic impurity local moment. In Fig. 5(a), we can see that the occupation number on the impurity site becomes larger in some regions, which corresponds to the case that the chemical potential is around the energy where VHS occurs. The double occupancy given in Fig. 5(b) shows similar behavior, and the local moment is determined by the competition between the occupation and the double occupancy. We can see that the local moment plotted in Fig. 5(c) becomes smaller in the same region. It is natural that,

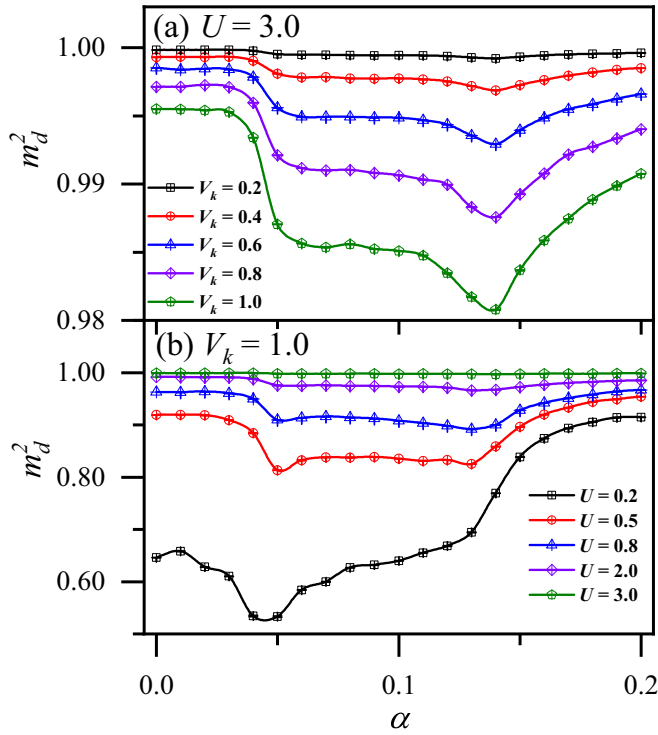


FIG. 6. The Hirsch-Fye quantum Monte Carlo (HFQMC) results of local moment squared for (a) $U = 3.0$ with various V_k values and (b) $V_k = 1.0$ for different U values. The chemical potential is $\mu = 1.0$, and the temperature is $k_B T = \frac{1}{32}$.

if the DOS at μ is large, the screening of the local magnetic impurity spin becomes stronger, so the local moment and the spin susceptibility shown in Fig. 5(d) are suppressed.

To check the tunability of local moment by α , we show the results of m_d^2 for different combinations of U and V_k in Fig. 6. The chemical potential is fixed at $\mu = 1.0$, and the temperature is $k_B T = \frac{1}{32}$. In Fig. 6(a), we choose $U = 3.0$ and change the hybridization strength V_k . For all values of V_k , we can find a dip of m_d^2 as we switch α . The reduction of local moment is caused by the increase of DOS due to the cubic Rashba term α . The change in m_d^2 is more obvious if V_k is larger. In Fig. 6(b), we show the local moment for different U values, while the hybridization is chosen as $V_k = 1.0$. We can still see a dip of m_d^2 as α varies, and the changes in local moment are more obvious for small U values. In general, for a magnetic impurity with strong V_k and relatively weak U , the local moment is largely tunable by switching the cubic Rashba SOC.

In the following, the spin-spin correlation between the local magnetic impurity and the conduction electron is studied for different combinations of α , V_k , and U values. The spin-spin correlation between the magnetic impurity and conduction electron can be calculated from the Green's functions as [108]

$$J_{zz}(\mathbf{r}) = \langle S_d^z S_c^z \rangle = \langle (g_{dd}^{\uparrow\uparrow} - g_{dd}^{\downarrow\downarrow}) \times (g_{cc}^{\uparrow\uparrow} - g_{cc}^{\downarrow\downarrow}) - g_{dc}^{\uparrow\uparrow} \cdot g_{cd}^{\uparrow\uparrow} - g_{dc}^{\downarrow\downarrow} \cdot g_{cd}^{\downarrow\downarrow} + g_{dc}^{\downarrow\downarrow} \cdot g_{cd}^{\uparrow\uparrow} + g_{dc}^{\uparrow\uparrow} \cdot g_{cd}^{\downarrow\downarrow} \rangle,$$

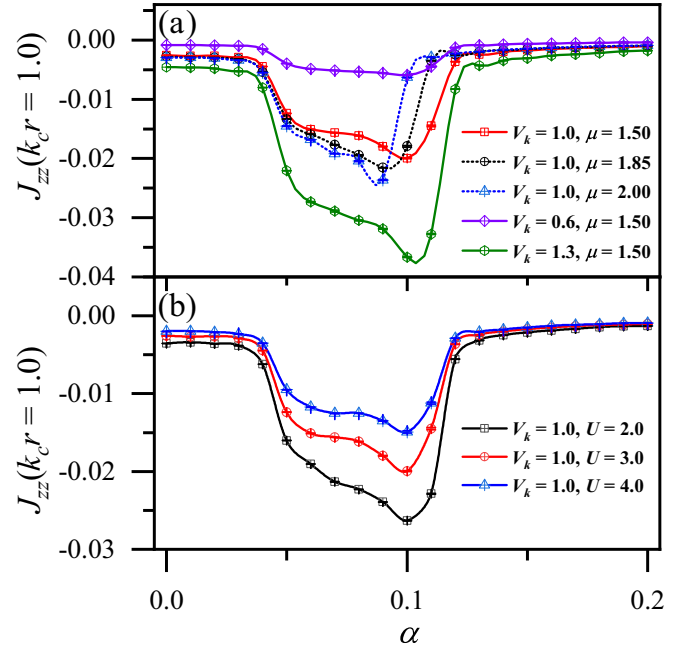


FIG. 7. The Hirsch-Fye quantum Monte Carlo (HFQMC) results of $J_{zz}(\mathbf{r} = \{1.0, 0\})$ with various combinations of V_k , μ , and U . (a) The results of $J_{zz}(\mathbf{r})$ vs α for (a) fixed value of $U = 3.0$, (b) for fixed $\mu = 1.5$ and $V_k = 1.0$. The temperature is chosen as $k_B T = \frac{1}{16}$.

$$\begin{aligned} J_{xx}(\mathbf{r}) &= \langle S_d^x S_c^x \rangle \\ &= \langle (g_{dd}^{\uparrow\downarrow} + g_{dd}^{\downarrow\uparrow}) \times (g_{cc}^{\uparrow\downarrow} + g_{cc}^{\downarrow\uparrow}) - g_{dc}^{\uparrow\downarrow} \cdot g_{cd}^{\uparrow\downarrow} - g_{dc}^{\downarrow\uparrow} \cdot g_{cd}^{\downarrow\uparrow} - g_{dc}^{\uparrow\uparrow} \cdot g_{cd}^{\downarrow\downarrow} - g_{dc}^{\downarrow\downarrow} \cdot g_{cd}^{\uparrow\uparrow} \rangle, \\ J_{yy}(\mathbf{r}) &= \langle S_d^y S_c^y \rangle \\ &= \langle -(g_{dd}^{\uparrow\downarrow} - g_{dd}^{\downarrow\uparrow}) \times (g_{cc}^{\uparrow\downarrow} - g_{cc}^{\downarrow\uparrow}) + g_{dc}^{\uparrow\downarrow} \cdot g_{cd}^{\uparrow\downarrow} + g_{dc}^{\downarrow\uparrow} \cdot g_{cd}^{\downarrow\uparrow} - g_{dc}^{\uparrow\uparrow} \cdot g_{cd}^{\downarrow\downarrow} - g_{dc}^{\downarrow\downarrow} \cdot g_{cd}^{\uparrow\uparrow} \rangle, \\ J_{xy}(\mathbf{r}) &= \langle S_d^x S_c^y \rangle \\ &= \langle i[(g_{dd}^{\uparrow\downarrow} + g_{dd}^{\downarrow\uparrow}) \times (g_{cc}^{\uparrow\downarrow} - g_{cc}^{\downarrow\uparrow}) - g_{dc}^{\uparrow\downarrow} \cdot g_{cd}^{\uparrow\downarrow} + g_{dc}^{\downarrow\uparrow} \cdot g_{cd}^{\downarrow\uparrow} + g_{dc}^{\uparrow\uparrow} \cdot g_{cd}^{\downarrow\downarrow} - g_{dc}^{\downarrow\downarrow} \cdot g_{cd}^{\uparrow\uparrow}] \rangle, \\ J_{xz}(\mathbf{r}) &= \langle S_d^x S_c^z \rangle \\ &= \langle (g_{dd}^{\uparrow\downarrow} + g_{dd}^{\downarrow\uparrow}) \times (g_{cc}^{\uparrow\uparrow} - g_{cc}^{\downarrow\downarrow}) + g_{dc}^{\uparrow\downarrow} \cdot g_{cd}^{\downarrow\downarrow} - g_{dc}^{\downarrow\uparrow} \cdot g_{cd}^{\uparrow\uparrow} - g_{dc}^{\uparrow\uparrow} \cdot g_{cd}^{\downarrow\downarrow} + g_{dc}^{\downarrow\downarrow} \cdot g_{cd}^{\uparrow\uparrow} \rangle, \\ J_{yz}(\mathbf{r}) &= \langle S_d^y S_c^z \rangle \\ &= \langle i[(g_{dd}^{\uparrow\downarrow} - g_{dd}^{\downarrow\uparrow}) \times (g_{cc}^{\uparrow\uparrow} - g_{cc}^{\downarrow\downarrow}) + g_{dc}^{\uparrow\downarrow} \cdot g_{cd}^{\downarrow\downarrow} + g_{dc}^{\downarrow\uparrow} \cdot g_{cd}^{\uparrow\uparrow} + g_{dc}^{\downarrow\downarrow} \cdot g_{cd}^{\uparrow\uparrow} - g_{dc}^{\uparrow\uparrow} \cdot g_{cd}^{\downarrow\downarrow} - g_{dc}^{\downarrow\downarrow} \cdot g_{cd}^{\uparrow\uparrow}] \rangle. \end{aligned}$$

We assume that the magnetic impurity is located at the origin of the coordinate, and \mathbf{r} is the position of the conduction electron. In Fig. 7, we show the results of $J_{zz}(\mathbf{r} = \{1.0, 0\})$ with various combinations of V_k , μ , and U . Given in Fig. 7(a) are the results of $J_{zz}(\mathbf{r})$ vs α for a fixed value of $U = 3.0$. For all parameters, we see that $J_{zz}(\mathbf{r})$ becomes stronger in a region as α increases. This region corresponds to the cases when the VHS emerges around the chemical potential μ . In general, the

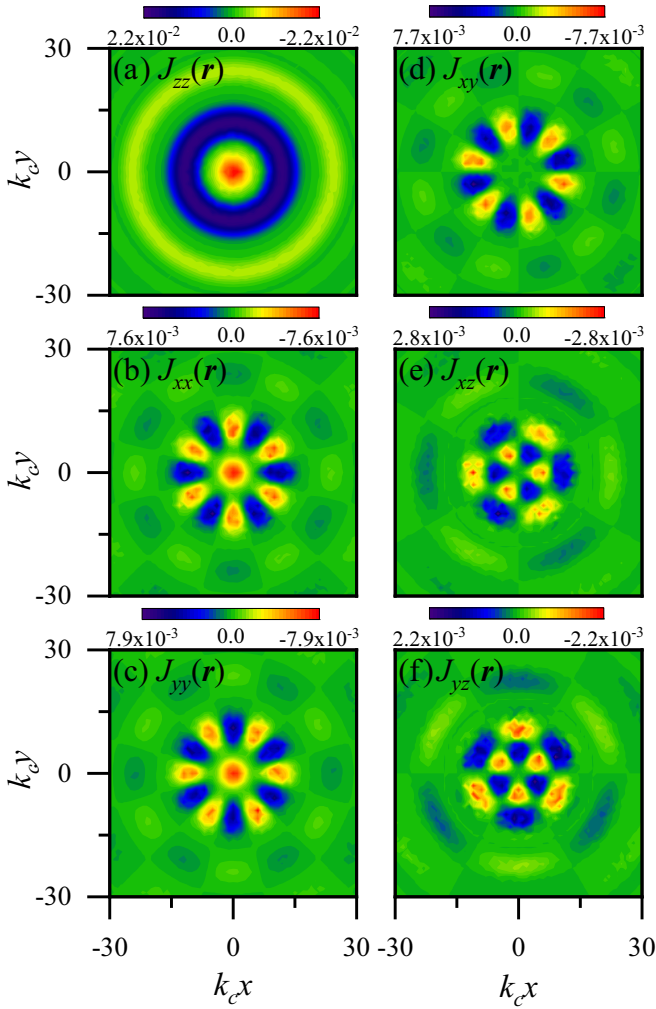


FIG. 8. The Hirsch-Fye quantum Monte Carlo (HFQMC) results of the spin-spin correlation between the magnetic impurity and the conduction electrons in the x - y plane. (a) $J_{zz}(\mathbf{r})$, (b) $J_{xx}(\mathbf{r})$, (c) $J_{yy}(\mathbf{r})$, (d) $J_{xy}(\mathbf{r})$, (e) $J_{xz}(\mathbf{r})$, and (f) $J_{yz}(\mathbf{r})$. The parameters are fixed as $\mu = 1.5$, $\alpha = 0.1$, $V_k = 1.0$, and $U = 3.0$, and the temperature is $k_B T = 1/16$.

values of $J_{zz}(\mathbf{r})$ grow with the hybridization strength V_k . In Fig. 7(b), we fix the chemical potential as $\mu = 1.5$, $V_k = 1.0$, and present the results for different U . For all values of U , we see similar behavior, that is, the increase of $J_{zz}(\mathbf{r})$ in a certain region of α . This indicates that the increase of spin-spin correlation is common for intermediate U values. Note that the relative magnitude of $J_{zz}(\mathbf{r})$ does not always decrease monotonically with U , and it depends on the choice of \mathbf{r} .

In Fig. 8, we show the HFQMC results of the spin-spin correlation between the magnetic impurity and the conduction electrons in the x - y plane. The parameters are fixed as $\mu = 1.5$, $\alpha = 0.1$, $V_k = 1.0$, and $U = 3.0$, and k_c is the momentum truncation. We can see that the HFQMC results of the spin-spin correlation exhibit basically the same symmetry as those obtained using the variational method, as in Fig. 3. Here, $J_{zz}(\mathbf{r})$ given in Fig. 8(a) is isotropic in the x - y plane. The other two diagonal components $J_{xx}(\mathbf{r})$ and $J_{yy}(\mathbf{r})$ given in Figs. 8(b) and 8(c) are sixfold rotational symmetric, and

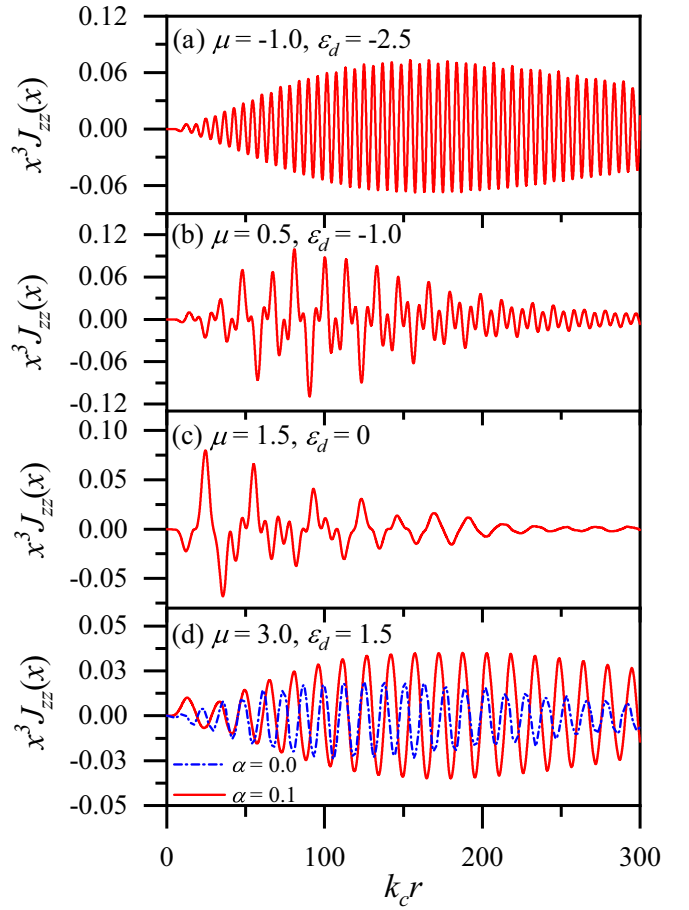


FIG. 9. The red solid lines show the results of $r^3 J_{zz}(\mathbf{r})$ along the x axis, while $\alpha = 0.1$ for (a) $\mu = -1.0$, (b) $\mu = 0.5$, (c) $\mu = 1.5$, and (d) $\mu = 3.0$. We use the symmetric case $\epsilon_d - \mu = -U/2$ in our Hirsch-Fye quantum Monte Carlo (HFQMC) simulations, so ϵ_d varies with respect to μ . The blue dashed line in (d) is the result for $10 \times r^3 J_{zz}(\mathbf{r})$ in a two-dimensional electron gas (2DEG) with $\alpha = 0$ for comparison. The parameters are $U = 3.0$, $V_k = 1.0$, and the temperature is $k_B T = \frac{1}{16}$.

$J_{xx}(\mathbf{r}) = J_{yy}[\mathcal{R}^z(\frac{\pi}{2})\mathbf{r}]$, which is consistent with the symmetry property of the host material, except for minor statistical errors caused in the QMC simulations. Here, $J_{xy}(\mathbf{r})$ given in Fig. 8(d) generally has the same symmetry property with that obtained from the variational method. Although $J_{xz}(\mathbf{r})$ and $J_{yz}(\mathbf{r})$ in Figs. 8(e) and 8(f) show opposite signs in comparison with the counterparts in Fig. 3, all of them follow the threefold rotational symmetry.

In Fig. 9, the red solid lines show the results of $r^3 J_{zz}(\mathbf{r})$ along the x axis while $\alpha = 0.1$. The parameters are $U = 3.0$, $V_k = 1.0$, and the temperature is $k_B T = \frac{1}{16}$. When $\alpha = 0.1$ and $\mu = -1.0$, as shown in Fig. 9(a), only the lower band ϵ_{k-} is involved in the screening process. We can see the spatial decay rate of the spin-spin correlation is about r^{-3} . As μ gradually increases, as in Figs. 9(b) and 9(c), both bands ϵ_{k-} and ϵ_{k+} take part in the Kondo screening, and the oscillation becomes more complicated. If $\mu = 3.0$, as given in Fig. 9(d), only the upper band ϵ_{k+} is responsible for the Kondo screening, and the decay rate of $J_{zz}(x, 0)$ is still proportional

to r^{-3} , with different period of oscillation. For comparison, the results of spin-spin correlation in a 2DEG for $\alpha = 0$ is plotted as the blue dashed line in Fig. 9(d). Note that, if $\alpha = 0$, the spin-spin correlation is much smaller than the $\alpha = 0.1$ case, so $r^3 J_{zz}(x, 0)$ is multiplied by 10 for clarity. Our results support the $1/r^3$ decay of the Kondo screening cloud at long distances, which is consistent with previous studies [39–41]. We can see that the spatial decay rate obtained by the HFQMC results is more reliable than those given by the variational method shown in Fig. 4. Our HFQMC results show that the decay rate of the spin-spin correlation remains essentially unchanged in the presence of the cubic Rashba term. However, the oscillation pattern and period are clearly affected by the cubic Rashba SOC.

IV. INDIRECT COUPLING BETWEEN TWO MAGNETIC IMPURITIES

Considering the indirect coupling between two magnetic impurities, one natural question shall be how the RKKY interaction is influenced by the cubic Rashba term. For simplicity, we assume that one impurity is located at the origin, and the other impurity is on the x axis with a distance R , as schematically plotted in Fig. 1(d). HFQMC returns the imaginary-time Green's functions $G_{jj'}^{ss'}(\mathbf{R}, \tau)$, where $j, j' = 1, 2$ mark the two magnetic atoms, and $s, s' = \uparrow, \downarrow$ are the spin indices. The spin-spin correlation between two magnetic impurities measures the RKKY interaction mediated by the conduction electrons. The nonzero components of the spin-spin correlation function along the x axis are [99]

$$\begin{aligned} \langle S_1^z S_2^z \rangle &= \langle S_1^x S_2^x \rangle \\ &= \langle (g_{11}^{\uparrow\uparrow} - g_{11}^{\downarrow\downarrow}) \times (g_{22}^{\uparrow\uparrow} - g_{22}^{\downarrow\downarrow}) - g_{12}^{\uparrow\uparrow} \cdot g_{21}^{\uparrow\uparrow} \\ &\quad - g_{12}^{\downarrow\downarrow} \cdot g_{21}^{\downarrow\downarrow} + g_{12}^{\uparrow\downarrow} \cdot g_{21}^{\downarrow\uparrow} + g_{12}^{\downarrow\uparrow} \cdot g_{21}^{\uparrow\downarrow} \rangle, \\ \langle S_1^y S_2^y \rangle &= \langle -(g_{11}^{\uparrow\downarrow} - g_{11}^{\downarrow\uparrow}) \times (g_{22}^{\uparrow\downarrow} - g_{22}^{\downarrow\uparrow}) + g_{12}^{\uparrow\downarrow} \cdot g_{21}^{\uparrow\downarrow} \\ &\quad + g_{12}^{\downarrow\uparrow} \cdot g_{21}^{\downarrow\uparrow} - g_{12}^{\uparrow\uparrow} \cdot g_{21}^{\downarrow\downarrow} - g_{12}^{\downarrow\downarrow} \cdot g_{21}^{\uparrow\uparrow} \rangle, \\ \langle S_1^x S_2^y \rangle &= -\langle S_1^y S_2^x \rangle \\ &= \langle (g_{11}^{\uparrow\downarrow} + g_{11}^{\downarrow\uparrow}) \times (g_{22}^{\uparrow\uparrow} - g_{22}^{\downarrow\downarrow}) + g_{12}^{\uparrow\downarrow} \cdot g_{21}^{\downarrow\downarrow} \\ &\quad - g_{12}^{\downarrow\uparrow} \cdot g_{21}^{\uparrow\uparrow} - g_{12}^{\uparrow\uparrow} \cdot g_{21}^{\downarrow\downarrow} + g_{12}^{\downarrow\downarrow} \cdot g_{21}^{\uparrow\uparrow} \rangle. \end{aligned}$$

In Fig. 10, we show the spin-spin correlation between the two magnetic impurities with respect to the distance R between them, and k_c is the momentum truncation. The parameters are chosen as $\alpha = 0.1$, $U = 3.0$ and $V_k = 1.0$, $k_B T = \frac{1}{8}$. We consider the symmetric case, with $\epsilon_d - \mu = -U/2$. Along the x axis, we can see that $\langle S_1^z S_2^z \rangle = \langle S_1^x S_2^x \rangle \neq \langle S_1^y S_2^y \rangle$. This is due to the cubic Rashba term α , without which all three components shall be the same. When $\alpha = 0.1$, the VHS emerges at energy value $\mu = 1.85$. Figures 10(a)–10(c) are listed in the order of increasing μ . Here, $\mu = 0.5$, given in Fig. 10(a), corresponds to relatively low DOS, while $\mu = 1.50$ and 1.85 , given in Figs. 10(b) and 10(c), are close to the energies where VHS occurs. We can see that the diagonal terms $\langle S_1^z S_2^z \rangle$ and $\langle S_1^x S_2^x \rangle$ are suppressed when $\mu = 0.5$. As μ approaches the VHS point, the DOS increases, and so do the diagonal terms $\langle S_1^z S_2^z \rangle$ and $\langle S_1^x S_2^x \rangle$. For all cases, the diagonal terms are positive and

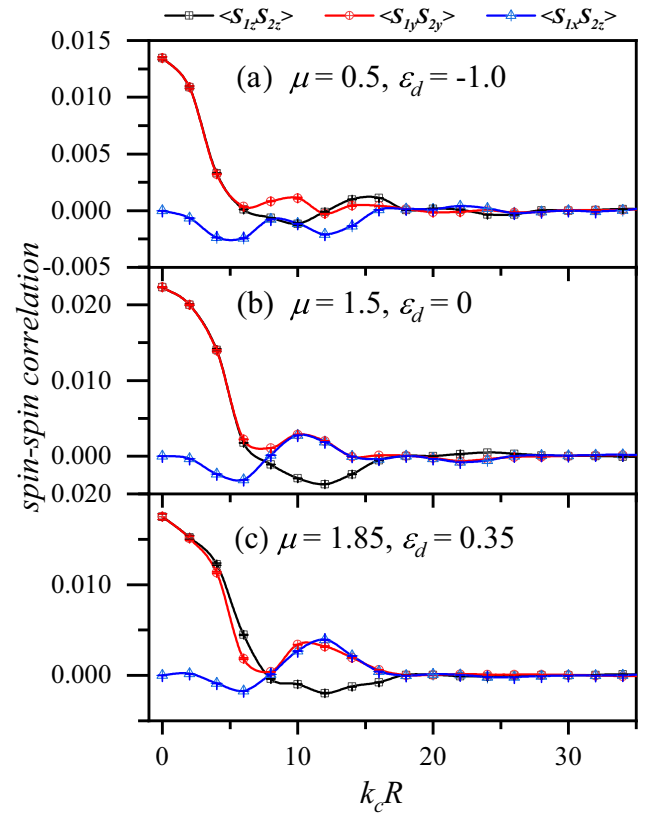


FIG. 10. The spin-spin correlation between two magnetic impurities with respect to the distance between them R . (a)–(c) are listed in the order of increasing μ , and $\epsilon_d - \mu = -U/2$. k_c is the momentum truncation, and the parameters are chosen as $U = 3.0$, $V_k = 1.0$, and $k_B T = 1/8$. The cubic Rashba spin-orbit coupling (SOC) term is $\alpha = 0.1$, and Van Hove singularity (VHS) occurs at energy 1.85.

dominant when the two impurities are close, indicating that the two magnetic impurities are ferromagnetically correlated, and the values oscillate and decay in space. The only nonzero off-diagonal term $\langle S_1^x S_2^y \rangle = -\langle S_1^y S_2^x \rangle$ also changes with respect to the values of μ . The off-diagonal terms correspond to the DM interaction [74–76], and it is a manifestation of the SOC in the host material. At distance $k_c R \sim 10$, the off-diagonal correlation $\langle S_1^x S_2^y \rangle$ is of the same order of magnitude as the diagonal terms.

V. CONCLUSIONS

In this paper, we apply the variational method and the HFQMC technique to study the influence of the k -cubic Rashba SOC on the correlation effects of magnetic impurities. The cubic Rashba SOC greatly alters the band structure and induces a VHS to the host material. The k -linear Rashba SOC can also cause the divergence of DOS, but the divergence occurs at the bottom of the bands. However, the VHS induced by the cubic Rashba SOC occurs in a very wide range of energy, and the single-impurity local moment becomes largely tunable, especially for strong V_k and relatively weak U . Both the variational method and the HFQMC simulations support the three- or sixfold rotational symmetry of the various components of spatial spin-spin correlation. This

unique feature is a manifestation of the cubic Rashba SOC and can possibly be used in experiments to distinguish the cubic Rashba SOC from the normal k -linear Rashba term. The HFQMC calculations show that the $1/r^3$ decay rate of this spin-spin correlation is essentially unchanged by the cubic Rashba SOC term α . Moreover, the RKKY couplings between two magnetic impurities display very complicated forms. In addition to the normal diagonal components, we still obtain the finite off-diagonal components, which correspond to the DM interaction between two magnetic impurities, and they become the same order of magnitude as the diagonal terms at distance $k_c R \approx 10$.

From the viewpoint of symmetry, once the cubic Rashba SOC appears, the linear Rashba SOC is allowed by symmetry; thus, both SOC's can coexist [22]. In this paper, the k -linear Rashba SOC is ignored to concentrate on the influence of cubic Rashba SOC on the magnetic impurities. Thus, our model Hamiltonian can be used to describe magnetic doping in systems such as strained-Ge/SiGe quantum wells [15,23] and SrTiO₃ singlecrystal surface [16] and heterostructures [24–27], in which the cubic Rashba SOC dominates. However, adding the k -linear Rashba SOC term will not change the symmetry property of the host; the system is still invariant under the operations $\mathcal{R}^z(\pi)$, $\mathcal{TR}^z(\pi/2)$, and \mathcal{M}_{xz} , \mathcal{M}_{yz} . Thus, the three- or sixfold rotational symmetry of the Kondo screening cloud shall still be valid in systems with coexisting linear and Rashba SOC's. Consequently, the Kondo screening cloud can still be used to identify the cubic Rashba SOC's in various systems, with or without the linear Rashba SOC.

Our study is based on a 2D continuous model. The major results given in this paper, such as the tunability of local moment by the cubic Rashba SOC's and the unique symmetries of Kondo screening cloud, are still applicable to a 2D lattice model with discrete momentum. So far, most cubic Rashba spin splittings are studied in 2D materials, such as quantum wells, surfaces, and interfaces. However, the investigation on cubic SOC's has been extended to bulk materials, and the Kondo screening in systems with cubic Rashba SOC in one-dimensional (1D) or three-dimensional systems might be an interesting issue. In a 1D system, the Kondo temperature takes the form $T_K \propto \exp[\pi\epsilon_d/N\Gamma]$ [109,110], where N is the degeneracy at the Fermi energy, and Γ is the effective hybridization. Thus, in a 1D (e.g., a 1D ring [111]) system with cubic Rashba SOC, we expect that the tunable correlation effect of magnetic impurities can still be observed, and we will probably investigate it in our future research.

ACKNOWLEDGMENTS

J.-H.S. acknowledges financial support from the Zhejiang Provincial Natural Science Foundation of China (Grant No. LY19A040003) and K. C. Wong Magna Fund in Ningbo University. D.-H.X. was supported by the NSFC (under Grants No. 12074108 and No. 12147102) and the Natural Science Foundation of Chongqing (Grant No. CSTB2022NSQ-MSX0568). L.C. was supported by the NSFC (under Grant No. 12174101) and the Fundamental Research Funds for the Central Universities (Grant No. 2022MS051).

-
- [1] G. Dresselhaus, *Phys. Rev.* **100**, 580 (1955).
 [2] E. Rashba, *Sov. Phys. Solid State* **2**, 1109 (1960).
 [3] F. J. Ohkawa and Y. Uemura, *J. Phys. Soc. Jpn.* **37**, 1325 (1974).
 [4] F. Vas'ko, *Pis'ma Zh. Eksp. Teor. Fiz.* **30**, 574 (1979).
 [5] Y. A. Bychkov and É. I. Rashba, *Pis'ma Zh. Eksp. Teor. Fiz.* **39**, 66 (1984).
 [6] G. Bihlmayer, O. Rader, and R. Winkler, *New J. Phys.* **17**, 050202 (2015).
 [7] A. Manchon, H. C. Koo, J. Nitta, S. M. Frolov, and R. A. Duine, *Nat. Mater.* **14**, 871 (2015).
 [8] G. Bihlmayer, P. Noël, D. V. Vyalikh, E. V. Chulkov, and A. Manchon, *Nat. Rev. Phys.* **4**, 642 (2022).
 [9] L. Gerchikov and A. Subashiev, *Sov. Phys. Semiconduct.* **26**, 73 (1992).
 [10] R. Winkler, *Spin-Orbit Coupling Effects in Two-Dimensional Electron and Hole Systems* (Springer, Berlin, Heidelberg, 2003), Vol. 191.
 [11] R. Winkler, *Phys. Rev. B* **62**, 4245 (2000).
 [12] J. Schliemann and D. Loss, *Phys. Rev. B* **71**, 085308 (2005).
 [13] O. Bleibaum and S. Wachsmuth, *Phys. Rev. B* **74**, 195330 (2006).
 [14] T. Ma and Q. Liu, *Phys. Rev. B* **73**, 245315 (2006).
 [15] R. Moriya, K. Sawano, Y. Hoshi, S. Masubuchi, Y. Shiraki, A. Wild, C. Neumann, G. Abstreiter, D. Bougeard, T. Koga *et al.*, *Phys. Rev. Lett.* **113**, 086601 (2014).
 [16] H. Nakamura, T. Koga, and T. Kimura, *Phys. Rev. Lett.* **108**, 206601 (2012).
 [17] M. Gmitra and J. Fabian, *Phys. Rev. B* **94**, 165202 (2016).
 [18] K. V. Shanavas, *Phys. Rev. B* **93**, 045108 (2016).
 [19] W. Lin, L. Li, F. Doğan, C. Li, H. Rotella, X. Yu, B. Zhang, Y. Li, W. S. Lew, S. Wang *et al.*, *Nat. Commun.* **10**, 3052 (2019).
 [20] D. C. Marinescu, *Phys. Rev. B* **96**, 115109 (2017).
 [21] A. Kundu, Z. B. Siu, and M. B. A. Jalil, *New J. Phys.* **24**, 123045 (2022).
 [22] H. J. Zhao, H. Nakamura, R. Arras, C. Paillard, P. Chen, J. Gosteau, X. Li, Y. Yang, and L. Bellaïche, *Phys. Rev. Lett.* **125**, 216405 (2020).
 [23] A. H. A. Hassan, R. J. H. Morris, O. A. Mironov, S. Gabani, A. Dobbie, and D. R. Leadley, *Appl. Phys. Lett.* **110**, 042405 (2017).
 [24] L. W. van Heeringen, A. McCollam, G. A. de Wijs, and A. Fasolino, *Phys. Rev. B* **95**, 155134 (2017).
 [25] H. Liang, L. Cheng, L. Wei, Z. Luo, G. Yu, C. Zeng, and Z. Zhang, *Phys. Rev. B* **92**, 075309 (2015).
 [26] C. S. Ho, W. Kong, M. Yang, A. Rusydi, and M. B. A. Jalil, *New J. Phys.* **21**, 103016 (2019).
 [27] L. W. van Heeringen, G. A. de Wijs, A. McCollam, J. C. Maan, and A. Fasolino, *Phys. Rev. B* **88**, 205140 (2013).
 [28] G. M. Minkov, A. A. Sherstobitov, A. V. Germanenko, O. E. Rut, V. A. Larionova, and B. N. Zvonkov, *Phys. Rev. B* **71**, 165312 (2005).

- [29] R. Winkler, H. Noh, E. Tutuc, and M. Shayegan, *Phys. Rev. B* **65**, 155303 (2002).
- [30] D. Y. Usachov, I. A. Nechaev, G. Poelchen, M. Güttler, E. E. Krasovskii, S. Schulz, A. Generalov, K. Kliemt, A. Kraiker, C. Krellner *et al.*, *Phys. Rev. Lett.* **124**, 237202 (2020).
- [31] D. Y. Usachov, M. Güttler, S. Schulz, G. Poelchen, S. Seiro, K. Kliemt, K. Kummer, C. Krellner, C. Laubschat, E. V. Chulkov *et al.*, *Phys. Rev. B* **101**, 245140 (2020).
- [32] S. Schulz, A. Y. Vyazovskaya, G. Poelchen, A. Generalov, M. Güttler, M. Mende, S. Danzenbächer, M. M. Otrokov, T. Balasubramanian, C. Polley *et al.*, *Phys. Rev. B* **103**, 035123 (2021).
- [33] S. Bhattacharya and S. Datta, *J. Phys.: Condens. Matter* **35**, 205501 (2023).
- [34] R. Arras, J. Gosteau, H. J. Zhao, C. Paillard, Y. Yang, and L. Bellaiche, *Phys. Rev. B* **100**, 174415 (2019).
- [35] J.-X. Xiong, S. Guan, J.-W. Luo, and S.-S. Li, *Phys. Rev. B* **105**, 115303 (2022).
- [36] P. W. Anderson, *Phys. Rev.* **124**, 41 (1961).
- [37] J. Kondo, *Prog. Theor. Phys.* **32**, 37 (1964).
- [38] K. G. Wilson, *Rev. Mod. Phys.* **47**, 773 (1975).
- [39] H. Ishii, *J. Low Temp. Phys.* **32**, 457 (1978).
- [40] V. Barzykin and I. Affleck, *Phys. Rev. B* **57**, 432 (1998).
- [41] L. Borda, *Phys. Rev. B* **75**, 041307(R) (2007).
- [42] C. P. Moca, I. Weymann, M. A. Werner, and G. Zaránd, *Phys. Rev. Lett.* **127**, 186804 (2021).
- [43] I. V. Borzenets, J. Shim, J. C. Chen, A. Ludwig, A. D. Wieck, S. Tarucha, H.-S. Sim, and M. Yamamoto, *Nature* **579**, 210 (2020).
- [44] J. Malecki, *J. Stat. Phys.* **129**, 741 (2007).
- [45] R. Žitko and J. Bonča, *Phys. Rev. B* **84**, 193411 (2011).
- [46] L. Isaev, D. F. Agterberg, and I. Vekhter, *Phys. Rev. B* **85**, 081107(R) (2012).
- [47] M. Zarea, S. E. Ulloa, and N. Sandler, *Phys. Rev. Lett.* **108**, 046601 (2012).
- [48] L. Chen, B. Hu, and R.-S. Han, *J. Phys.: Condens. Matter* **30**, 025601 (2018).
- [49] A. Wong, S. E. Ulloa, N. Sandler, and K. Ingersent, *Phys. Rev. B* **93**, 075148 (2016).
- [50] L. Chen, J. Sun, H.-K. Tang, and H.-Q. Lin, *J. Phys.: Condens. Matter* **28**, 396005 (2016).
- [51] L. Li, J.-H. Sun, Z.-H. Wang, D.-H. Xu, H.-G. Luo, and W.-Q. Chen, *Phys. Rev. B* **98**, 075110 (2018).
- [52] Y. Luh, *Acta Phys. Sin.* **21**, 75 (1965).
- [53] H. Shiba, *Prog. Theor. Phys.* **40**, 435 (1968).
- [54] A. Rusinov, *Sov. Phys. JETP* **29**, 1101 (1969).
- [55] E. Hudson, K. Lang, V. Madhavan, S. Pan, H. Eisaki, S. Uchida, and J. Davis, *Nature* **411**, 920 (2001).
- [56] A. Yazdani, C. M. Howald, C. P. Lutz, A. Kapitulnik, and D. M. Eigler, *Phys. Rev. Lett.* **83**, 176 (1999).
- [57] E. W. Hudson, S. H. Pan, A. K. Gupta, K.-W. Ng, and J. C. Davis, *Science* **285**, 88 (1999).
- [58] S. Pan, E. Hudson, K. Lang, H. Eisaki, S. Uchida, and J. Davis, *Nature* **403**, 1476 (2000).
- [59] W.-F. Tsai, Y.-Y. Zhang, C. Fang, and J. Hu, *Phys. Rev. B* **80**, 064513 (2009).
- [60] Y. Bang, H.-Y. Choi, and H. Won, *Phys. Rev. B* **79**, 054529 (2009).
- [61] A. Akbari, I. Eremin, and P. Thalmeier, *Phys. Rev. B* **81**, 014524 (2010).
- [62] G.-Q. Zha and Y.-Y. Jin, *Europhys. Lett.* **120**, 27002 (2018).
- [63] Y.-W. Guo, W. Li, and Y. Chen, *Front. Phys.* **12**, 127403 (2017).
- [64] J. D. Sau and E. Demler, *Phys. Rev. B* **88**, 205402 (2013).
- [65] Z.-G. Fu, P. Zhang, Z. Wang, and S.-S. Li, *J. Phys.: Condens. Matter* **24**, 145502 (2012).
- [66] L. Chen, Y.-L. Zhang, and R.-S. Han, *J. Phys.: Condens. Matter* **31**, 505603 (2019).
- [67] R. Chen, B. Zhou, and D.-H. Xu, *Phys. Rev. B* **97**, 155152 (2018).
- [68] R. Chirila, C. P. Moca, and I. Weymann, *Phys. Rev. B* **87**, 245133 (2013).
- [69] X.-Y. Feng, W.-Q. Chen, J.-H. Gao, Q.-H. Wang, and F.-C. Zhang, *Phys. Rev. B* **81**, 235411 (2010).
- [70] X.-Y. Feng and F.-C. Zhang, *J. Phys.: Condens. Matter* **23**, 105602 (2011).
- [71] T. Kasuya, *Prog. Theor. Phys.* **16**, 45 (1956).
- [72] M. A. Ruderman and C. Kittel, *Phys. Rev.* **96**, 99 (1954).
- [73] K. Yosida, *Phys. Rev.* **106**, 893 (1957).
- [74] H. Imamura, P. Bruno, and Y. Utsumi, *Phys. Rev. B* **69**, 121303(R) (2004).
- [75] D. F. Mross and H. Johannesson, *Phys. Rev. B* **80**, 155302 (2009).
- [76] J.-J. Zhu, D.-X. Yao, S.-C. Zhang, and K. Chang, *Phys. Rev. Lett.* **106**, 097201 (2011).
- [77] J. E. Hirsch and R. M. Fye, *Phys. Rev. Lett.* **56**, 2521 (1986).
- [78] O. Gunnarsson and K. Schönhammer, *Phys. Rev. Lett.* **50**, 604 (1983).
- [79] C. M. Varma and Y. Yafet, *Phys. Rev. B* **13**, 2950 (1976).
- [80] J.-H. Sun, D.-H. Xu, F.-C. Zhang, and Y. Zhou, *Phys. Rev. B* **92**, 195124 (2015).
- [81] J.-H. Sun, L.-J. Wang, X.-T. Hu, L. Li, and D.-H. Xu, *Phys. Rev. B* **97**, 035130 (2018).
- [82] D. Ma, H. Chen, H. Liu, and X. C. Xie, *Phys. Rev. B* **97**, 045148 (2018).
- [83] L.-J. Wang, X.-T. Hu, L. Li, D.-H. Xu, J.-H. Sun, and W.-Q. Chen, *Phys. Rev. B* **99**, 235108 (2019).
- [84] X.-R. Yang, Z.-Z. Huang, W.-S. Wang, and J.-H. Sun, *Chin. Phys. B* **30**, 067103 (2021).
- [85] J. Simonin and R. Allub, *Phys. Rev. Lett.* **74**, 466 (1995).
- [86] M. E. Simon and C. M. Varma, *Phys. Rev. B* **60**, 9744 (1999).
- [87] A. V. Rozhkov and D. P. Arovas, *Phys. Rev. B* **62**, 6687 (2000).
- [88] Z.-Z. Huang, X.-T. Peng, W.-S. Wang, and J.-H. Sun, *Chin. Phys. B* **31**, 107101 (2022).
- [89] F. D. M. Haldane and P. W. Anderson, *Phys. Rev. B* **13**, 2553 (1976).
- [90] B. Uchoa, V. N. Kotov, N. M. R. Peres, and A. H. Castro Neto, *Phys. Rev. Lett.* **101**, 026805 (2008).
- [91] R. M. Fye and J. E. Hirsch, *Phys. Rev. B* **38**, 433 (1988).
- [92] R. M. Fye, J. E. Hirsch, and D. J. Scalapino, *Phys. Rev. B* **35**, 4901 (1987).
- [93] J. E. Hirsch and H. Q. Lin, *Phys. Rev. B* **35**, 4943 (1987).
- [94] N. Bulut, K. Tanikawa, S. Takahashi, and S. Maekawa, *Phys. Rev. B* **76**, 045220 (2007).
- [95] F. M. Hu, T. Ma, H.-Q. Lin, and J. E. Gubernatis, *Phys. Rev. B* **84**, 075414 (2011).
- [96] J. Sun, F. Hu, H. Tang, W. Guo, and H. Lin, *J. Appl. Phys.* **113**, 17B515 (2013).
- [97] J. Sun, F. Hu, H. Tang, and H. Lin, *Int. J. Mod. Phys. B* **27**, 1362039 (2013).

- [98] J.-H. Sun and H.-K. Tang, *Chin. Phys. B* **27**, 077502 (2018).
- [99] J. Sun, L. Chen, and H.-Q. Lin, *Phys. Rev. B* **89**, 115101 (2014).
- [100] F. M. Hu, T. O. Wehling, J. E. Gubernatis, T. Frauenheim, and R. M. Nieminen, *Phys. Rev. B* **88**, 045106 (2013).
- [101] M. Zarea and S. E. Ulloa, *Phys. Rev. B* **73**, 165306 (2006).
- [102] P. Kim, K. T. Kang, G. Go, and J. H. Han, *Phys. Rev. B* **90**, 205423 (2014).
- [103] H. Liu, E. Marcellina, A. R. Hamilton, and D. Culcer, *Phys. Rev. Lett.* **121**, 087701 (2018).
- [104] C. Xiao, Y. Liu, Z. Yuan, S. A. Yang, and Q. Niu, *Phys. Rev. B* **100**, 085425 (2019).
- [105] S. Y. Liu and X. L. Lei, *Phys. Rev. B* **72**, 155314 (2005).
- [106] L. Karwacki, A. Dyrdał, J. Berakdar, and J. Barnaś, *Phys. Rev. B* **97**, 235302 (2018).
- [107] A. C. Hewson, *The Kondo Problem to Heavy Fermions* (Cambridge University Press, Cambridge, 1997).
- [108] J. E. Gubernatis, J. E. Hirsch, and D. J. Scalapino, *Phys. Rev. B* **35**, 8478 (1987).
- [109] M.-S. Choi, R. López, and R. Aguado, *Phys. Rev. Lett.* **95**, 067204 (2005).
- [110] J. S. Lim, M.-S. Choi, M. Y. Choi, R. López, and R. Aguado, *Phys. Rev. B* **74**, 205119 (2006).
- [111] S. Smirnov, *Phys. Rev. B* **79**, 134403 (2009).